Nonlinear Dyn (2007) 48:97–114
DOI 10.1007/s11071-006-9076-2

ORIGINAL ARTICLE

Nonlinear stochastic analysis of subharmonic response of a shallow cable

Q. Zhou · J. W. Larsen · S. R. K. Nielsen · W. L. Qu

Received: 16 November 2005 / Accepted: 1 March 2006 / Published online: 5 December 2006
© Springer Science + Business Media B.V. 2006

Abstract The paper deals with the subharmonic response of a shallow cable due to time variations of the chord length of the equilibrium suspension, caused by time varying support point motions. Initially, the capability of a simple nonlinear two-degree-of-freedom model for the prediction of chaotic and stochastic subharmonic response is demonstrated upon comparison with a more involved model based on a spatial finite difference discretization of the full nonlinear partial differential equations of the cable. Since the stochastic response quantities are obtained by Monte Carlo simulation, which is extremely time-consuming for the finite difference model, most of the results are next based on the reduced model. Under harmonical varying support point motions the stable subharmonic motion consists of a harmonically varying component in the equilibrium plane and a large subharmonic out-of-plane component, producing a trajectory at the midpoint of shape as an infinity sign. However, when the harmonical variation of the chordwise elongation is replaced by a narrow-banded Gaussian excitation with the same standard deviation and a centre frequency equal to the circular frequency of the harmonic excitation, the slowly varying phase of the excitation implies that the phase difference between the in-plane and out-of-plane displacement components is not locked at a fixed value. In turn this implies that the trajectory of the displacement components is slowly rotating around the chord line. Hence, a large subharmonic response component is also present in the static equilibrium plane. Further, the time variation of the envelope process of the narrow-banded chordwise elongation process tends to enhance chaotic behaviour of the subharmonic response, which is detectable via extreme sensitivity on the initial conditions, or via the sign of a numerical calculated Lyapunov exponent. These effects have been further investigated based on periodic varying chord elongations with the same frequency and standard deviation as the harmonic excitation, for which the amplitude varies in a well-defined way between two levels within each period. Depending on the relative magnitude of the high and low amplitude phase and their relative duration the onset of chaotic vibrations has been verified.

Keywords Shallow cables · Subharmonic response · Stochastic vibrations · Chaotic vibrations · Monte Carlo simulation

Q. Zhou (✉) · J. W. Larsen · S. R. K. Nielsen
Department of Civil Engineering, Aalborg University, Sohngaardsholmsvej 57, DK-9000 Aalborg, Denmark
e-mail: drzhouqiang@hotmail.com

Q. Zhou · W. L. Qu
Hubei Key Laboratory of Roadway Bridge and Structure Engineering, Wuhan University of Technology, Wuhan 430070, P.R. China

1 Introduction

Cable systems are of great interest in a wide range of applications in civil engineering to supply both support

and stability to large structures. Typically, cables used as support of cable-stayed bridges, masts and TV-towers are characterized by a sag-to-chord-length ratio below say 0.01, which means that the natural frequencies for the in-plane and the out-of-plane eigenmodes are pairwise close. The primarily external excitation of such cables is caused by the motion of the support points of the cable rather than by external distributed dynamic wind or aeroelastic loads. Especially, the component of the support point motion along the chord of the equilibrium suspension introduces both additive and parametric excitation terms in the nonlinear modal equations of motion due to the elongation and shortening of the chord length.

Dangerous situations arise when the chord elongation is harmonically varying with a circular frequency ω_0 in certain disjoint intervals. Especially, when ω_0 is about twice the first out-of-plane circular eigenfrequency ω_1 of the cable, large subharmonic vibrations with the circular frequency $\omega_0/2$ may take place, also known as 2:1 internal resonances. It turns out that the single mode in-plane subharmonic of the order 2 is unstable for arbitrarily small excitation amplitudes. Instead a coupled vibration occurs, in which large subharmonic vibrations out of the static equilibrium plane take place with the circular $\omega_0/2$ frequency, whereas the in-plane vibrations are harmonically varying with the circular frequency ω_0, and with a relatively small amplitude. The out-of-plane component is brought forward by nonlinear couplings, and has a well-defined phase lead to the in-plane harmonic component. The indicated phase locking between the two vibration components produces a trajectory of shape like an infinity sign as shown in Fig. 1a. When $\omega_0 \approx \frac{1}{2}\omega_1$ or $\omega_0 \approx \frac{2}{3}\omega_1$, similar coupled in-plane and out-of-plane resonances may occur. These cases, which are known as superharmonic responses of the orders 1:2 and 2:3, were investigated by Nielsen and Kirkegaard [1]. The effect of harmonic forced support motions has also been considered by Perkins [2], who obtained analytical solutions based on a first-order perturbation analysis of a two degree-of-freedom (DOF) model for coupled in-plane and out-of-plane responses. The emphasis was placed on cables with relatively large sag-to-chord-length ratios to analyze 2:1 internal resonances. Pinto da Costa et al. [3] studied oscillations in the static equilibrium plane of bridge stay cables subjected to periodic motions of the deck and/or towers using a Galerkin method. El-Attar et al. [4] evaluated the nonlinear cable response to multiple periodic support excitations with different phase using a reduced 2DOF model. Rega and co-workers [5] had an in-depth investigation about nonlinear multimodal interaction and chaotic motion of the cable under the forced excitation using multimode models theoretically and experimentally.

In reality the supported structure is performing narrow-banded stochastic vibrations with a centre frequency ω_0 close to the fundamental eigenfrequency. Hence, the chord elongation will also be narrow-banded stochastic varying. Larsen and Nielsen [6] studied the harmonic stochastic response of a shallow cable, i.e. the case where the centre frequency ω_0 of the chord elongation process is close to ω_1. Under these frequency conditions up to three stable motions may coexist, and the triggering mechanism for transition between these three attractors under narrow-banded Gaussian excitation was investigated. The subject of the present paper is to perform a similar investigation

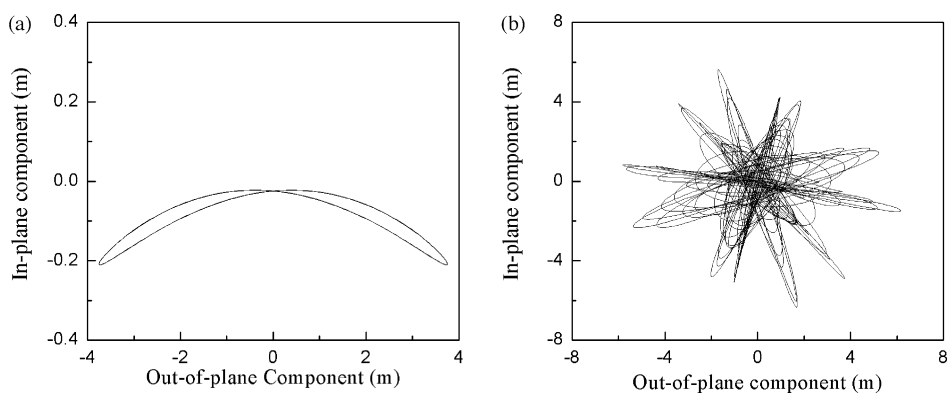

Fig. 1 Trajectory at the mid-span of the cable. (a) Harmonic chord elongation. (b) Stochastic chord elongation

in case of stochastic subharmonic excitation, where the centre frequency fulfils $\omega_0 \approx 2\omega_1$.

The subharmonic responses under condition of comparable stochastic and harmonic varying chord elongations are qualitatively very different as shown in Fig. 1, where typical trajectories at the mid-span of the cable have been depicted. The slowly time variation of the amplitude of the chord elongation process implies a slowly variation of the amplitudes of the in-plane and out-of-plane components. Most important, the phase between the two components is no longer locked at a certain value but becomes slowly varying with time. This variation causes the trajectory of the response to rotate slowly around the chord line, introducing a large subharmonic response component also in the static equilibrium plane. In the paper this effect has been demonstrated by replacing the harmonical excitation with a periodic chord elongation signal, which may vary between two levels within each period in a controlled manner, so the standard deviation and centre frequency of the signal is identical to those of the stochastic signal. Further, it is demonstrated that the time variation of the envelope of the chord elongation process may enhance the tendency to chaotic behaviour of the response. Again, this is analyzed by the use of the equivalent periodic excitation. The referential mechanical model is based on a spatial finite difference deviation of the governing nonlinear partial differential equation. The stochastic analysis is carried out based on Monte Carlo simulation, which makes such a model rather time consuming. For this reason, the suitability of a simple two DOF model is demonstrated for prediction of both stochastic subharmonic response and the onset of chaotic behaviour of the cable.

2 Theory

2.1 Equations of motion

The dynamic behaviour of the cable is described in the Cartesian (x, y, z) coordinate system shown in Fig. 2. The x-axis is placed along the chord, and the static equilibrium state is placed in the x-y plane. The equilibrium state is caused by the component $g\cos\theta$ of the acceleration of gravity g in the y direction, where θ denotes the angle of the chord line with the horizontal plane. The cable is subjected to support excitations $u(0, t)$ and $u(l, t)$ along the chord line, so the elongation of the chord line becomes $u(l, t) - u(0, t)$. Because the profile is shallow, the longitudinal displacement component of the cable can be considered ignorable. Neglecting the flexural rigidity of the cable and assuming a parabolic static equilibrium of the cable, the nonlinear equations of motion of the cable can be expressed as [7]

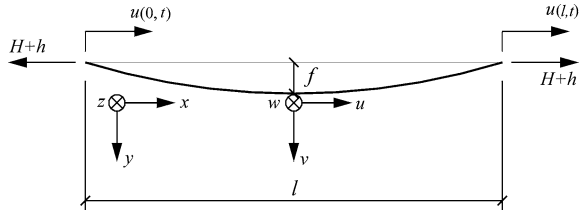

Fig. 2 Cable in static equilibrium configuration

$$(H+h)\frac{\partial^2 v}{\partial x^2} - \frac{mg\cos\theta}{H}h - m\frac{\partial^2 v}{\partial t^2} = 0 \tag{1}$$

$$(H+h)\frac{\partial^2 w}{\partial x^2} - m\frac{\partial^2 w}{\partial t^2} = 0 \tag{2}$$

where H and h are the components of the static and dynamic tension in the x direction, v and w are the dynamic displacement components in the y and z directions measured from the static equilibrium position. l is the initial cable chord length, m denotes the mass per unit length, and t is the time.

Retaining up to cubic geometric nonlinear terms, h is given by

$$h = \frac{EA}{L_e}\left(u(l) - u(0) + 8\frac{f}{l^2}\int_0^l v\,dx + \frac{1}{2}\int_0^l \left(\frac{\partial v}{\partial x}\right)^2 dx + \frac{1}{2}\int_0^l \left(\frac{\partial w}{\partial x}\right)^2 dx\right) \tag{3}$$

where E and A indicate the elastic modulus and cross sectional area of the cable, L_e denotes the so-called effective cable length, and f is the sag at the mid-span, given as

$$L_e \approx l\left[1 + 8\left(\frac{f}{l}\right)^2\right], \quad f = \frac{mgl^2\cos\theta}{8H} \tag{4}$$

In what follows emphasize will be on the case where the chord wise elongation causes simultaneous resonance in the lowest in-plane and out-of-plane

modes. Under subharmonic excitation the second in-plane mode will be at resonance. However, this mode will not contribute to the linear displacement response at the cable mid-point because the modal load is zero. All other modes may be considered small, and may be disregarded approximately [6]. Therefore, the dynamic displacements of the cable in the vertical and transverse directions are modeled in the form

$$v(x,t) = \Phi_2(x)q_2(t), \quad w(x,t) = \Phi_1(x)q_1(t) \tag{5}$$

where $\Phi_2(x)$ and $\Phi_1(x)$ are the first in-plane and out-of-plane linear undamped eigen-modes of the cable based on the parabolic equilibrium suspension, and $q_1(t)$ and $q_2(t)$ are the corresponding modal coordinates. The eigenmodes are normalized to unit at the mid-point, so $q_1(t)$ and $q_2(t)$ are measures of the dynamic response at this position.

Inserting (5) into (1)–(3), and using the relevant orthogonality properties, the coupled ordinary differential equations for the pertinent modal coordinates $q_1(t)$ and $q_2(t)$ can be expressed as (more details see [6])

$$\ddot{q}_1 + 2\zeta_1\omega_1\dot{q}_1 + \omega_1^2(1+e(t))q_1 + \beta_1 q_1 q_2 + q_1\left(\gamma_1 q_1^2 + \gamma_2 q_2^2\right) = 0 \tag{6}$$

$$\ddot{q}_2 + 2\zeta_2\omega_2\dot{q}_2 + \omega_2^2(1+\alpha e(t))q_2 + \beta_2 q_1^2 + \beta_3 q_2^2 + q_2\left(\gamma_3 q_1^2 + \gamma_4 q_2^2\right) = -\eta e(t) \tag{7}$$

where ω_1 and ω_2 are the first out-of-plane and in-plane circular eigenfrequencies of the cable, and ζ_1 and ζ_2 denote appropriate modal damping ratios, respectively. $e(t)$ is a nondimensional representation of the chord length elongation given by

$$e(t) = \frac{EA}{H}\frac{u(l,t)-u(0,t)}{L_e} = \frac{EA}{H}\frac{\Delta u}{L_e} \tag{8}$$

The eigenmodes, as well as the introduced coefficients in (6) and (7), are listed in Appendix A. The relevance of the reduced models (6) and (7) under subharmonic excitation will be investigated by comparison to a nonlinear spatial finite difference (FD) discretization of the partial differential equations of motion (1) and (2) under both deterministic and stochastic chordwise elongations. A detailed description of the FD model has been given in [8].

Assume that $e(t)$ is harmonically varying with the circular frequency $\omega_0 \approx 2\omega_1$, the amplitude e_0 and the phase a

$$e(t) = e_0\cos(\omega_0 t + a) \tag{9}$$

Possible periodic solutions to (6) and (7) either take place in the static equilibrium plane, in which case $q_1(t) \equiv 0$, or are coupled in-plane and out-of-plane motions. Retaining only the dominating harmonic components, the in-plane subharmonic response has the Fourier expansion

$$q_2(t) = A_2 + B_2\cos\left(\frac{\omega_0}{2}t + b_2\right) \tag{10}$$

where A_2 represents a small static drift. The corresponding truncated Fourier expansion of the coupled subharmonic motion reads

$$q_1(t) = B_1\cos\left(\frac{\omega_0}{2}t + b_1\right) \tag{11a}$$

$$q_2(t) = A_2 + C_2\cos(\omega_0 t + c_2) \tag{11b}$$

As seen the in-plane component of the coupled motion is harmonically varying with a non-zero mean value, and only the out-of-plane motion is subharmonic. The amplitudes and phases of the anticipated solutions (10) and (11) may be obtained by the method of harmonic balance [9]. The results have been indicated in Appendix B.

Two solutions exist to (10) of which only one is stable. The stable solution is related with the following phase locking, see (B4)

$$a - 2b_2 \approx \pi \tag{12}$$

However, the indicated subharmonic response only exists as long as the out-of-plane component is fixed. Else, the stable attractor is given by the coupled motion (11) with the phase locking, see (B10)

$$c_2 - 2b_1 \approx \pi, \quad a - 2b_1 \approx \pi, \tag{13}$$

The trajectory at the mid-point obtained by (11) with the analytical determined amplitudes and phase (B10) has been shown with a dashed signature in Fig. 5.

2.2 Models for the chord elongation

The stochastic model for the nondimensional chord elongation $e(t)$ is obtained from a second-order filtration of Gaussian white noise [6]

$$\ddot{e} + 2\mu\omega_0\dot{e} + \omega_0^2 e = \sqrt{2\mu\omega_0^3}e_0 W(t) \tag{14}$$

where μ is a band width parameter, ω_0 is the circular centre frequency of the filter, and e_0 is a nondimensional scaling parameter for the output. $W(t)$ is a zero-mean unit intensity Gaussian white noise process defined by the auto-covariance function

$$\kappa_{WW}(\tau) = E\left[W(t)W(t+\tau)\right] = \delta(\tau) \tag{15}$$

where $\delta(\tau)$ signifies the Dirac impulse function. The normalization (14) insures that the standard deviation σ_e of $e(t)$ becomes

$$\sigma_e = \frac{\sqrt{2}}{2}e_0 \tag{16}$$

Hence, the narrow-banded stochastic excitation is comparable to the harmonic excitation (9) with the amplitude e_0 and the circular frequency ω_0.

The following so-called Van der Pol transformation between $(\,e(t)\;\dot{e}(t)\,)$ and $(\,r(t)\;a(t)\,)$ applies to any zero mean random process, [10]

$$\begin{aligned} e(t) &= r(t)\cos\left(\omega_0 t + a(t)\right), \\ \dot{e}(t) &= -\omega_0 r(t)\sin\left(\omega_0 t + a(t)\right) \end{aligned} \tag{17}$$

For a narrow-banded Gaussian process, the envelope process $r(t)$ and the phase process $a(t)$ are slowly varying with time. At a given instant of time $r(t)$ and $a(t)$ are independent stochastic variables, $r(t)$ is Rayleigh distributed with the parameter $\sigma^2 = \frac{e_0^2}{2}$, and $a(t)$ is uniformly distributed in the instant $[0, 2\pi]$. The essential difference between (9) and the first Equation (17) is that the phase now is varying with time. For this reason the phase difference $c_2 - 2b_1$ in the truncated Fourier expansion (11) will also be slowly varying with time with the implication that the trajectory of the displacement component is slowly rotating around the chord line.

The state vector of the combined dynamic system of the reduced mechanical model (6), (7) and the filter Equation (14), has the dimension 6. In principle the stochastic analysis of the problem can be achieved via numerical integration of the related Fokker-Planck equation. Although the stationary solution to the Fokker-Planck equation with a state vector of dimension 6 is within reach, see Wagner and Wedig [11], the present problem is non-stationary due to the parametric terms. This increases the calculation time significantly, since the solution effort at each time step is equivalent to that of the stationary problem. In any case this approach is out of the question for the multidimensional FD-model. Further, because the probability density function (PDF) of $q_1(t)$ has a narrow significant peak at $q_1 = 0$, and hence differs significantly from Gaussian distribution, moment methods (stochastic linearization, cumulant-neglect closure etc.) will not converge sufficiently fast either. Therefore, the stochastic analysis is performed by Monte Carlo simulation. The samples of the stochastic support motion are generated using a broad-banded broken line process as an equivalent white noise input process [12]. Response statistics will be obtained based on ergodic sampling using a single sufficiently long sample curve of the elongation process to ensure reliable estimates.

Typical realizations of the chord elongation process have been shown in Fig. 3 for the band width parameter $\mu = 0.001$ and $\mu = 0.01$, and with the circular centre frequency chosen as $\omega_0 = 2\omega_1$. The realizations have been indicated with time normalized to the centre period $T_0 = 2\pi/\omega_0$. Further, the sample curves of the corresponding energy envelope process have been shown in the figures with a dashed signature. The significantly faster time variation of the envelope process $r(t)$ for $\mu = 0.01$ than for $\mu = 0.001$ as shown in Fig. 3 turns out to be important for an enhanced tendency of chaotic behaviour. In order to investigate this effect in a controlled way a periodic chord elongation function as shown in Fig. 4 is introduced. The amplitude variation of the chord elongation within a period is divided between a high amplitude phase with the amplitude $e_{\max}$ and duration αT_0, followed by a low amplitude phase with the amplitude $e_{\min}$ and duration βT_0. Hence, the period of the excitation becomes $T = (\alpha + \beta)T_0$. The

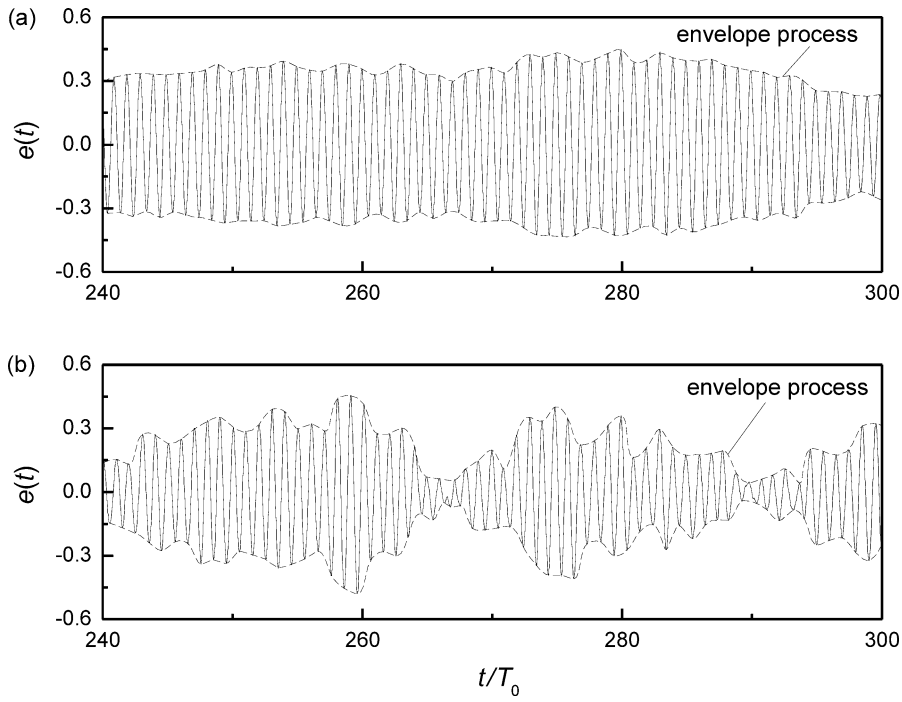

Fig. 3 Realizations of stochastic chord elongation process, $e_0 = 0.30$, $\omega_0 = 2\omega_1$. (a) $\mu = 0.001$. (b) $\mu = 0.01$

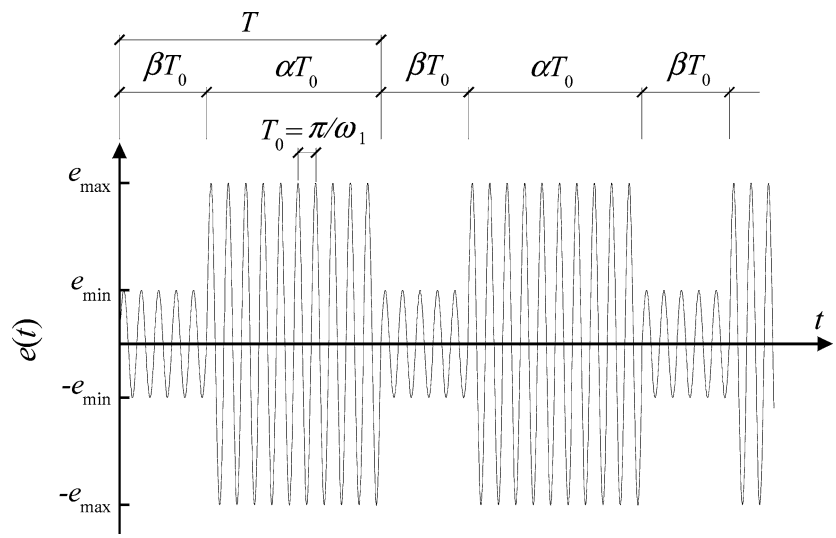

Fig. 4 Periodic chord elongation function

band width parameter μ specifies the clump size of high amplitude oscillations in the stochastic signal. Keeping β at a fixed value, the corresponding parameter in the periodic signal is given by the fraction α/β. The standard deviation (RMS value) of the chord elongation becomes

$$\sigma_e = \frac{\sqrt{2}}{2} e_0 \sqrt{\frac{\alpha\left(\frac{e_{\max}}{e_0}\right)^2 + \beta\left(\frac{e_{\min}}{e_0}\right)^2}{\alpha + \beta}} \tag{18}$$

Upon comparison with the equivalent harmonical and stochastic excitations, α, β, and the fractions $e_{\max}/e_0$ and $e_{\min}/e_0$ should be chosen so the square root is equal to one.

3 Verification of the reduced 2DOF model for subharmonic response analysis

The nonlinear FD model applies a nonlinear Newmark scheme as time integration, involving iterations

towards dynamical equilibrium at each time step, which makes this model very time consuming in Monte Carlo simulations. Hence, it is favourable to use the reduced mechanical models (6) and (7) for the stochastic subharmonic analysis. However, the adequacy of the reduced model for this purpose needs to be verified at first.

The considered cable in this verification phase and the following investigations are the longest stay in the cable-stayed bridge across the Oresund between Denmark and Sweden, for which the following data applies: $EA = 2.17 \times 10^9$ N, $H = 5.5 \times 10^6$ N, $l = 260.0$ m, $m = 81.05$ kg/m, and $\theta = 30.4^\circ$. The circular frequencies of the fundamental in-plane and out-of-plane modes become $\omega_2 = 3.20$ rad/s and $\omega_1 = 3.148$ rad/s, respectively. The modal damping ratios of modes are set to $\zeta_1 = \zeta_2 = 1.0\%$.

At first, the chord elongation is assumed to be harmonically varying with the circular frequency $\omega_0 = 2\omega_1$ and the nondimensional amplitude $e_0 = 0.30$. Fig. 5 shows the trajectories at the mid-point of the cable obtained by the FD model, numerical integration of the reduced systems (6) (7), and the truncated Fourier expansion (11) of the solutions of (6) (7). It can be seen that the out-of-plane component is accurately predicted by all these models. Moreover, the numerical solutions of (6) (7) and the analytic solution based on the truncated Fourier series (11) are in good agreement. However, the peak-to-peak value of the in-plane motion predicted by the reduced model is about 0.14 m, while the FD model predicts about 0.16 m. The difference is primarily caused by the linear response of the second

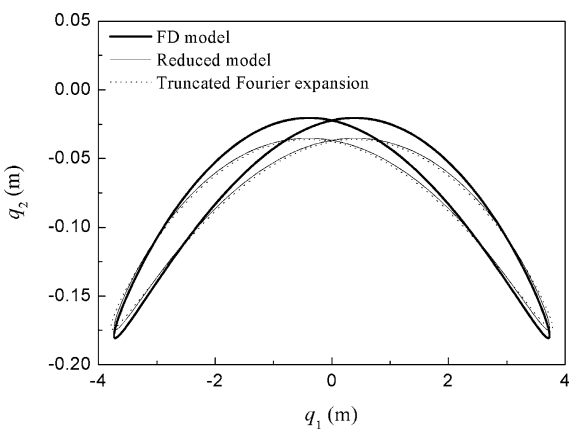

Fig. 5 Harmonic varying chord elongation. Trajectory at the mid-point. $e_0 = 0.30$, $\omega_0/\omega_1 = 2$

symmetric in-plane mode with the circular eigenfrequency $\omega_6 \approx 3\omega_1$. This is because the corresponding modal coordinate $q_6(t)$ is far from resonance during the subharmonic excitation with $\omega_0 \approx 2\omega_1$. Hence, the said contribution to the subharmonic response at the mid-point becomes almost linear. In principle the first antisymmetric mode with the circular eigenfrequency $\omega_4 = 2\omega_1$ will be at resonance. However, the modal load corresponding to the right-hand side of Equation (7) will be zero, so this mode will only be excited via nonlinear coupling terms. Moreover, the corresponding eigenmode $\Phi_4(x)$ has a node at the mid-point, so this mode is not affecting the subharmonic response at the mid-point at all. Several periods of oscillation have been depicted in the figure, and the thin lined trajectories suggest that the response is not chaotic.

Next, the time variation of the chord elongation is assumed to be periodic. In this case the cable response may be predictable or chaotic depending on the excitation parameters. Fig. 6 shows the results for the parameter values $e_0 = 0.30$, $e_{\max}/e_0 = 1.225$, $e_{\min}/e_0 = 0.5$, $\alpha/\beta = 1.5$, $\beta = 10$ and $\omega_0/\omega_1 = 2$. The indicated parameters imply that the square root in (12) is equal to one. Hence, the specified excitation is comparable to the harmonic case considered in Fig. 5 with respect to variance and frequency contents. As seen in Fig. 6a the displacement response predicted by the FD model and the reduced model are quite similar. In both cases the response becomes periodic and predictable with the period $T_r = 50T_0$, which is the twice of the period of the excitation. The corresponding trajectories at the mid-span as shown in Fig. 6b are also in good agreement. Obviously, these trajectories are qualitatively and quantitatively completely different from the corresponding trajectories of the harmonic case shown in Fig. 5. First of all a significant in-plane response component of the same magnitude as the out-of-plane component is present. Due to the indicated calibration of the chord elongation model, this variation can only be attributed to the amplitude variation of the periodic model. Fig. 7 shows the phase difference between the in-plane and out-of-plane displacement components at the mid-point with the FD model. In Fig. 7, the time series of $q_1(t)$ and $q_2(t)$ have been shown in the same plot. First, it is noticed that both modal coordinates are dominated by the subharmonic component with the circular frequency $\frac{\omega_0}{2}$, and that the amplitude of $q_2(t)$ is comparable to that of $q_1(t)$. Further, the phase difference between $q_1(t)$ and $q_2(t)$ is slowly and monotonously increasing with

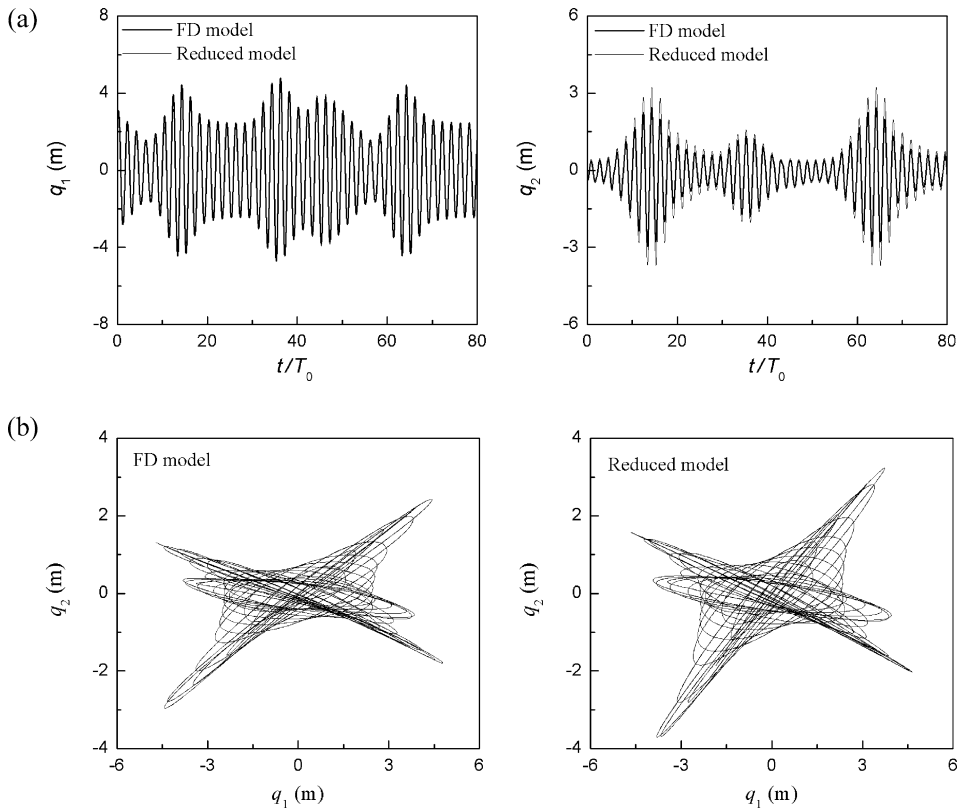

Fig. 6 Periodic varying chord elongation. $e_0 = 0.30$, $e_{max}/e_0 = 1.225$, $e_{min}/e_0 = 0.5$, $\alpha/\beta = 1.5$, $\beta = 10$, $\omega_0/\omega_1 = 2$. (a) Displacements at the mid-point. (b) Trajectories at the mid-point

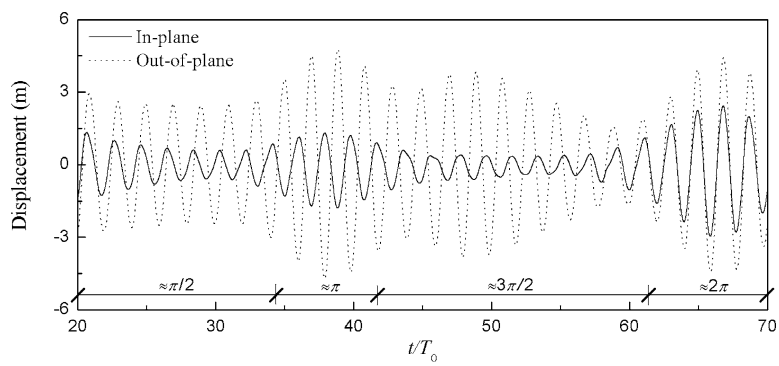

Fig. 7 Periodic varying chord elongation, FD model. Variation phase difference between in-plane and out-of-plane displacement component. $e_0 = 0.30$, $e_{max}/e_0 = 1.225$, $e_{min}/e_0 = 0.5$, $\alpha/\beta = 1.5$, $\beta = 10$, $\omega_0/\omega_1 = 2$

time, without locking at a specific value, as is the case for harmonically varying chord elongation. When the phase difference is close to $\pm\frac{\pi}{2}$ the trajectory of the cable at the mid-point has the shape of an ellipse, whereas a phase difference of $\pm\pi$ produces straight lines. Both of these trajectories are visible in Fig. 6b.

Next, in Fig. 8 the same system is analyzed with the slightly changed excitation parameters $e_0 = 0.30$, $e_{max}/e_0 = 1.392$, $e_{min}/e_0 = 0.5$, $\alpha/\beta = 0.8$, $\beta = 10$ and $\omega_0/\omega_1 = 2$. The variance and the frequency ω_0 of the excitation are unchanged. However, the period has been reduced from $T = 25T_0$ to $T = 18T_0$, indicating a somewhat more rapid variation between high and low amplitude excitations. The response time series as predicted by the two mechanical models are shown in Fig. 8a. As seen these deviate substantially, suggesting that either the FD model or the reduced model produces chaotic response in this case. This has been verified in Fig. 8b,

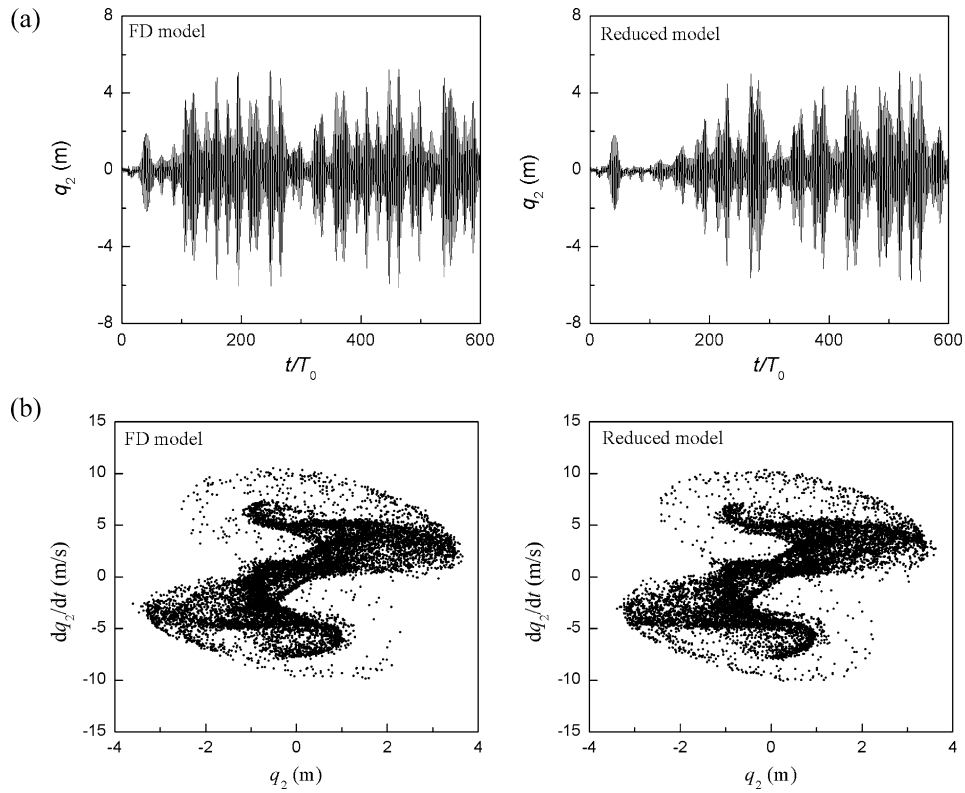

Fig. 8 Periodic varying chord elongation. $e_0 = 0.30$, $e_{max}/e_0 = 1.392$, $e_{min}/e_0 = 0.5$, $\alpha/\beta = 0.8$, $\beta = 10$, $\alpha_0/\alpha_1 = 2$. (a) In-plane displacement at the mid-point. (b) Poincaré maps of in-plane response

which shows quite similar Poincaré maps based on the excitation period $T = 18T_0$ for the in-plane response. Based on this and similar investigations it is concluded that the FD model and the reduced model either both produce a chaotic (non-predictable) response, or an ordered (predicable) response at the mid-point.

Finally, the suitability of the 2DOF system for predicting the stochastic subharmonic displacement response of the cable has been demonstrated in Fig. 9 by comparison of the predictions of the FD model and the reduced model for the same chord elongation time series. The centre frequency of the excitation process is kept constant at $\omega_0 = 2\omega_1$, whereas e_0 and μ are varied. Only the in-plane displacement has been shown. Fig. 9a displays the results for $e_0 = 0.15$, $\mu = 0.005$, corresponding to a narrow-banded excitation with relatively small variance. As seen the response is completely predictable, and both models give almost the same quantitative result. Next, in Figs. 9b and c the parameters have been changed to $e_0 = 0.45$, $\mu = 0.005$ and $e_0 = 0.15$, $\mu = 0.02$, respectively. In both cases the predictions of the two models are completely different, suggesting that the response to the given chord elongation realization is chaotic. Hence, the chaotic behaviour may occur either at large variance levels, or at large band width values. The latter effect is related to the rapid change of the envelope process as explained in relation to Fig. 3. The chaotic behaviour in Fig. 9c has been further investigated in Fig. 10 by imposing slightly different initial value, $q_1(0) = 1.00$ m and $q_1(0) = 1.01$ m, on the considered mechanical models. In both cases all other initial values are set to zero. Further, the same sample curve of the chord elongation process has been used as in Fig. 9c. As seen from the figures, both models show extreme sensibility on the initial values.

From the indicated analysis it is concluded that the reduced model performs qualitatively and quantitatively like the more involved FD model as long as the response is predictable. Further, both models produce a chaotic subharmonic stochastic response, whenever the predictions are no longer qualitatively and quantitatively in agreement. In addition, the difference between the reduced model and the FD scheme when the

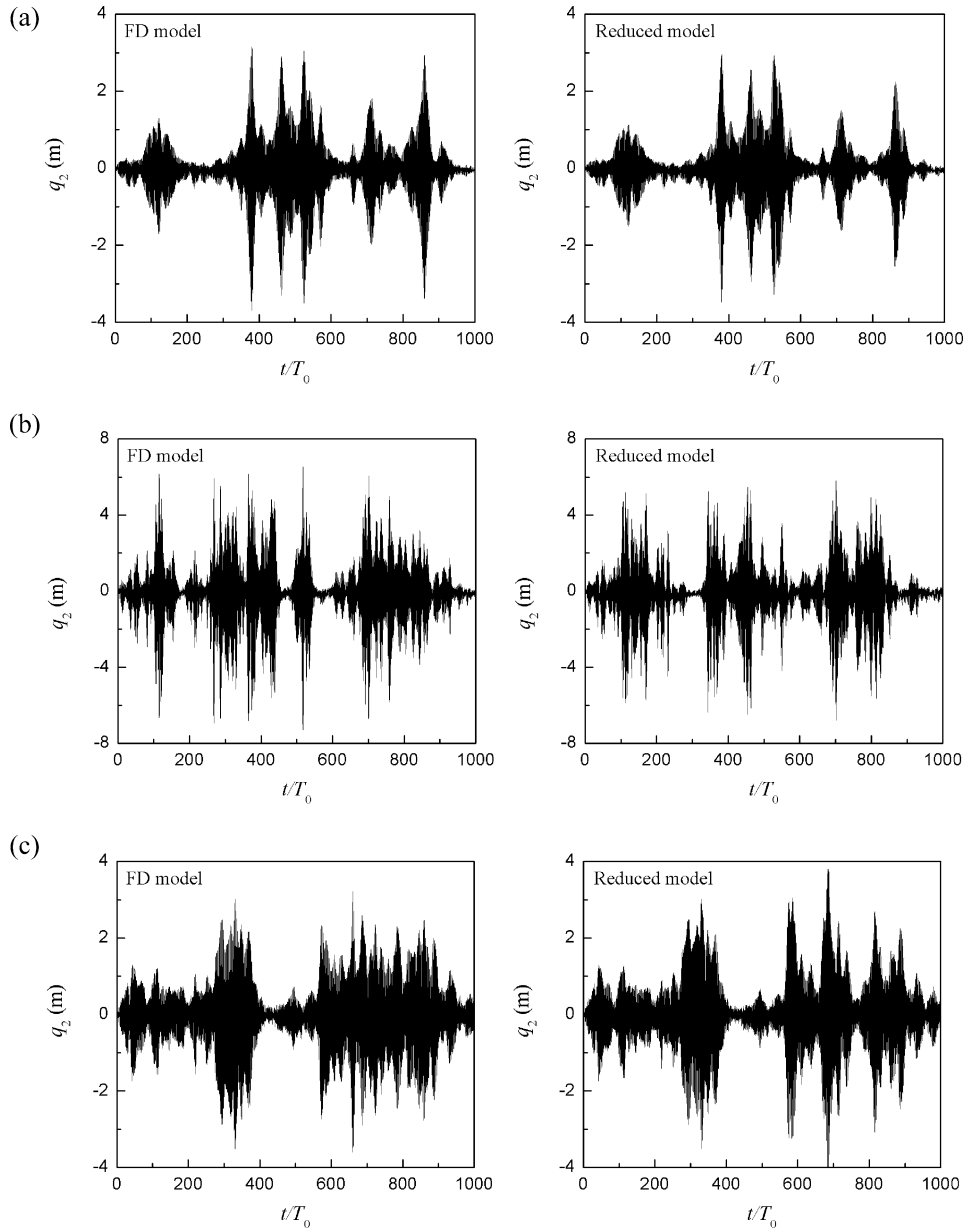

Fig. 9 Stochastic chord elongation. In-plane displacement response at the mid-point. $\omega_0/\omega_1 = 2$. (a) $e_0 = 0.15$, $\mu = 0.005$. (b) $e_0 = 0.45$, $\mu = 0.005$. (c) $e_0 = 0.15$, $\mu = 0.02$

responses are chaotic suggests that other modes may be activated within the more relaxed FD procedure.

The response under stochastic subharmonic excitation will be characterized by variances, power spectral densities (PSD), and probability density functions of the modal coordinates $q_1(t)$ and $q_2(t)$. In order to use the reduced model for stochastic analysis, it is necessary to compare these quantities predicted by the two models. In Fig. 11 the predicted variances have been compared for the case $e_0 = 0.30$ as a function of μ. Despite the models behave chaotic for some values of μ, the variances are in good agreement. Similar observations have been made for the estimates of the PSDs and PDFs. Hence, it may be concluded that the reduced model is sufficiently accurate for stochastic subharmonic analysis of shallow cables, and the following analysis will be based on this model.

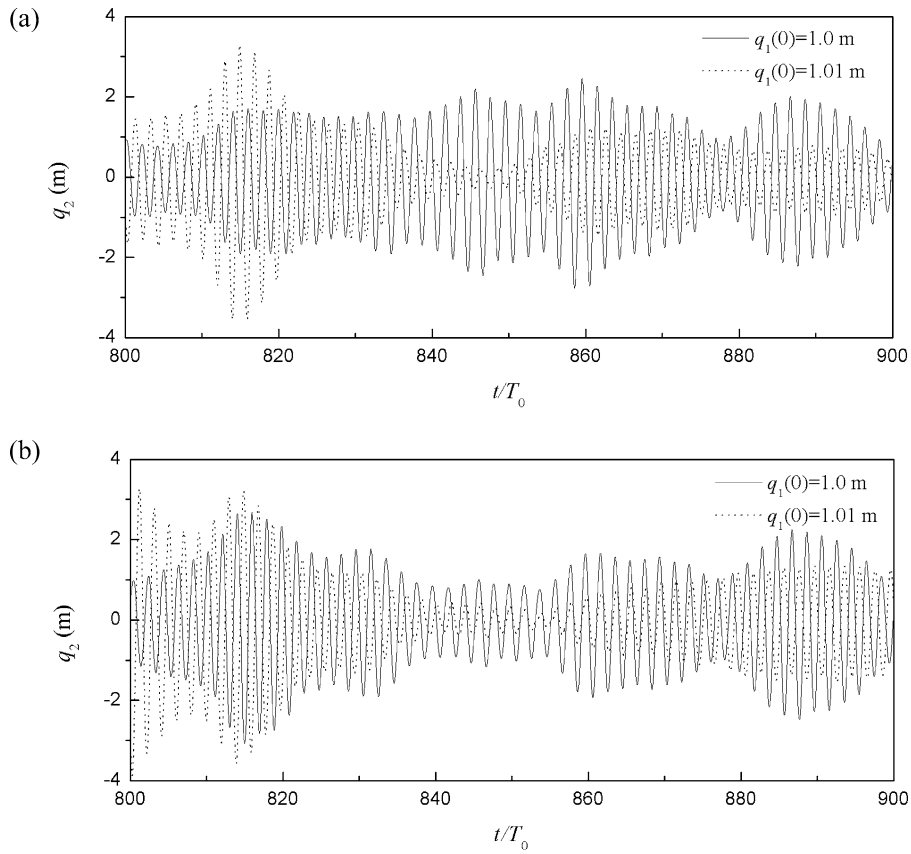

Fig. 10 Stochastic chord elongation. Dependence of in-plane displacement at the mid-point on initial value. $e_0 = 0.15$, $\mu = 0.02$, $\omega_0/\omega_1 = 2$. (a) FD model. (b) Reduced model

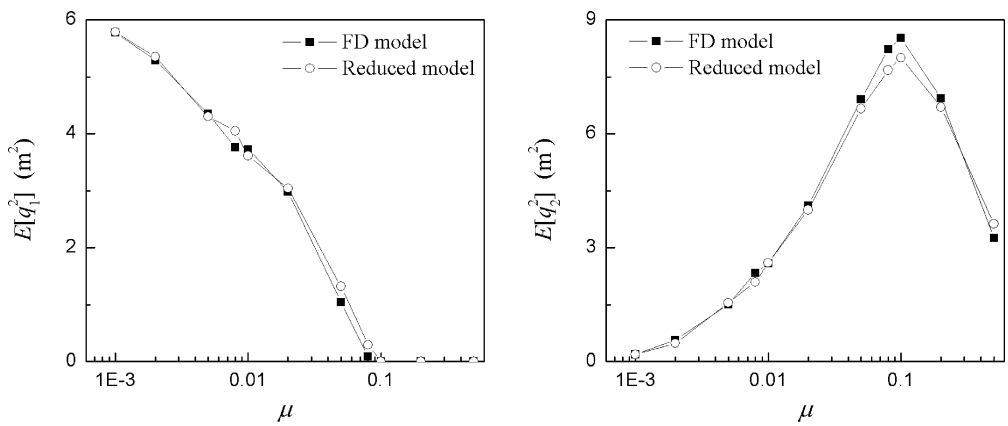

Fig. 11 Stochastic chord elongation. Variance response at the mid-point. $e_0 = 0.30$, $\omega_0/\omega_1 = 2$

4 Chaotic response

In order to further analyze chaotic subharmonic cable vibration, the largest Lyapunov exponent is calculated by the algorithm by Wolf et al. [13]. A positive Lyapunov exponent indicates exponential growth of a normed perturbation of the state vector $z^T(t) = [q_1(t) \quad q_2(t) \quad \dot{q}_1(t) \quad \dot{q}_2(t)]$, revealing chaotic behaviour. Fig. 12 shows the largest Lyapunov exponent as a function of the amplitude e_0 under harmonically

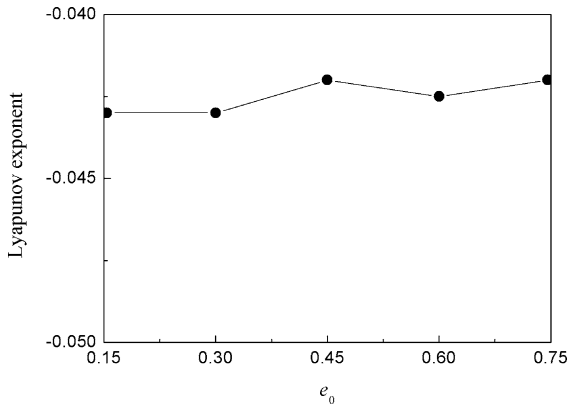

Fig. 12 Harmonic varying chord elongation. Variation of Lyapunov exponent with $e_0 \cdot \omega_0/\omega_1 = 2$

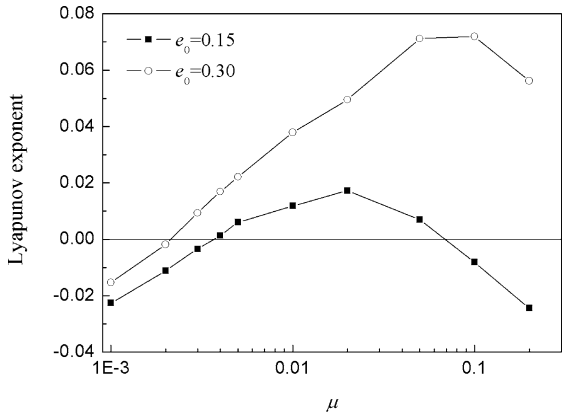

Fig. 13 Stochastic chord elongation. Variation of Lyapunov exponent with $\mu \cdot \omega_0/\omega_1 = 2$

varying chord elongations with the circular frequency $\omega_0 = 2\omega_1$. Since the Lyapunov exponents are negative in all cases, it is concluded that subharmonic vibrations under harmonic excitation are non-chaotic for any realistic value of the amplitude e_0.

Next, the chord elongation is assumed to be narrow-banded stochastic. Fig. 13 shows the calculated Lyapunov exponents as a function of the band width parameter μ for the characteristic amplitudes $e_0 = 0.15$ and $e_0 = 0.30$. At very small values of μ the excitation has very slowly varying amplitudes, and resembles a harmonic excitation. Under these conditions the Lyapunov exponent is negative in both cases in agreement with the findings in Fig. 12. As μ is increased the Lyapunov exponent becomes positive corresponding to chaotic response. As mentioned this can be attributed to the increased variability of the envelope process of the excitation. It is also seen from the figure that larger values of the characteristic amplitude e_0 enhances the tendency to chaotic behaviour of the response. As seen for $e_0 = 0.15$, non-chaotic behaviour occur at both small and large values of μ. Although the complete variation is not shown in the figure, a similar behaviour takes place for $e_0 = 0.30$.

5 Stochastic subharmonic analysis

Figure 14 shows the time series of the displacement response at the mid-point under stochastic chord elongation with the center frequency $\omega_0 = 2\omega_1$ for various values of the band width parameter. Fig. 14a shows the results for μ=0.001 corresponding to the excitation time series shown in Fig. 3a. As seen the in-plane response is significantly smaller than the out-of-plane response, indicating that the trajectory of the stochastic subharmonic response is randomly varying, but qualitatively in agreement with the one shown in Fig. 5 for the case of harmonic excitation. Fig. 14b shows the corresponding results in the moderate narrow-banded case $\mu = 0.01$ corresponding to the excitation time series in Fig. 3b. In this case significant in-plane subharmonic vibrations are persistently present, which are caused by the faster variability of the envelope process of the chord elongation. Finally, Fig. 14c shows the results, where the band width parameter is further increased to $\mu = 0.1$. Then, the out-of-plane component has disappeared, and only the in-plane subharmonic response remains. This suggests that the out-of-plane stochastic subharmonic component will only be stable for band width parameter below a critical value $\mu = \mu_c(e_0)$, which may depend on the characteristic excitation amplitude e_0. Further, that the in-plane subharmonic response, which is unstable under harmonical varying excitation, exists under stochastic excitation with band width parameter $\mu > \mu_c(e_0)$.

This issue has been further investigated in Fig. 15, where the variance of the mid-point displacement response is shown as a function of μ for specified values of e_0. It is seen that the variance $E[q_1^2]$ of the subharmonic response of the out-of-plane component decreases monotonously with μ for a given value of e_0, until the critical value $\mu = \mu_c(e_0)$ is reached. Beyond this point only the in-plane subharmonic component exists. As seen, $\mu_c(e_0)$ is an increasing function of e_0. Simultaneously with the decrease of $E[q_1^2]$, the variance

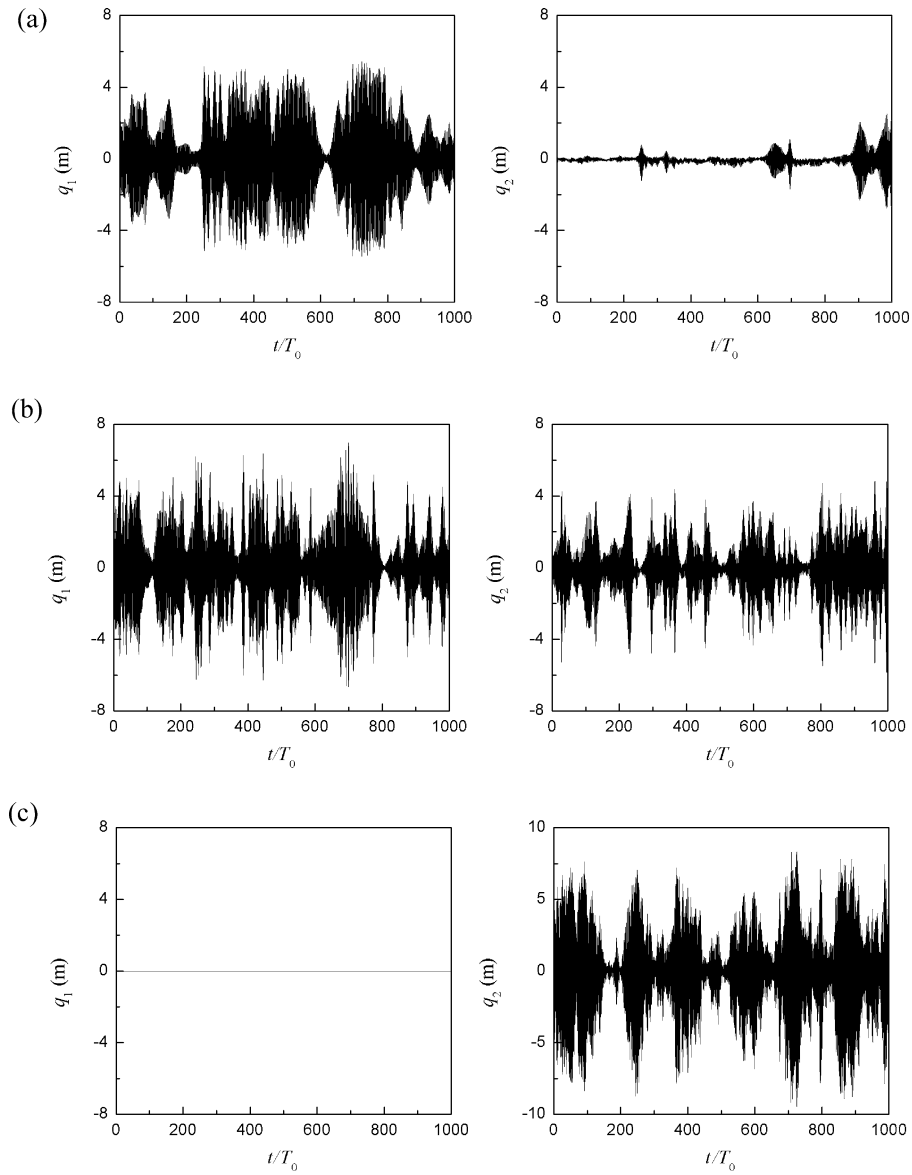

Fig. 14 Stochastic chord elongation. Displacement response at the mid-point. $e_0 = 0.30$, $\omega_0/\omega_1 = 2$. (a) $\mu = 0.001$. (b) $\mu = 0.01$. (c) $\mu = 0.1$

of the in-plane component increases in magnitude, and a maximum value is reached at the bifurcation point $\mu = \mu_c$ of the out-of-plane variance response.

Figures 16 and 17 show the variation of the power spectral density (PSD) for discrete values of e_0 and μ. Fig. 16 shows the results, when the characteristic amplitude is fixed at the value $e_0 = 0.30$, and the band width parameter is varied. The indicated spectral density for $\mu = 0.1$ for the out-of-plane component should merely be considered as numerical noise, since this component is unstable in this case. As seen the peak frequency and half-band width of the spectra of both the in-plane and the out-of-plane displacements increase with μ. Further, a secondary spectral peak in the PSD of $q_2(t)$ at $\omega \approx 2\omega_1 = \omega_0$ is noticed. This peak is completely dominating, corresponding to the harmonic amplitude C_2 in the truncated Fourier expansion (11b), under purely harmonically varying chord elongations. Figure 17 shows the corresponding spectral densities for the band width parameter $\mu = 0.01$,

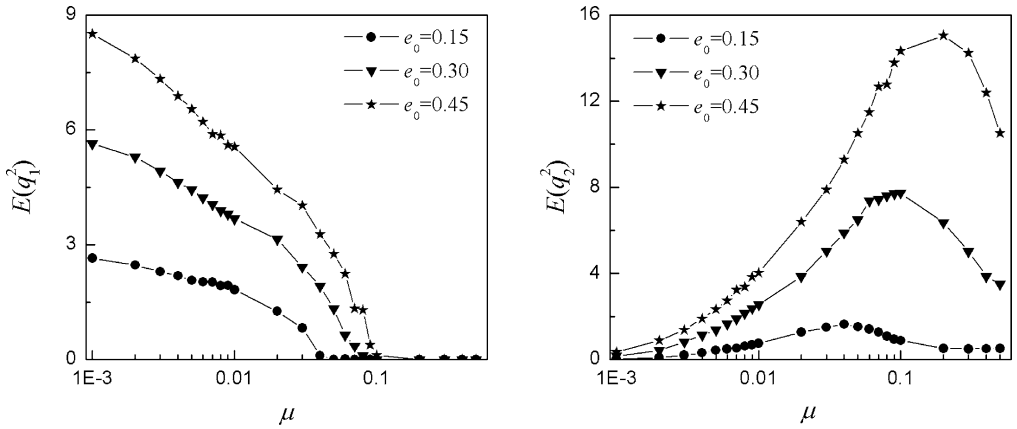

Fig. 15 Stochastic chord elongation. Variance response at the mid-point. $\omega_0/\omega_1 = 2$

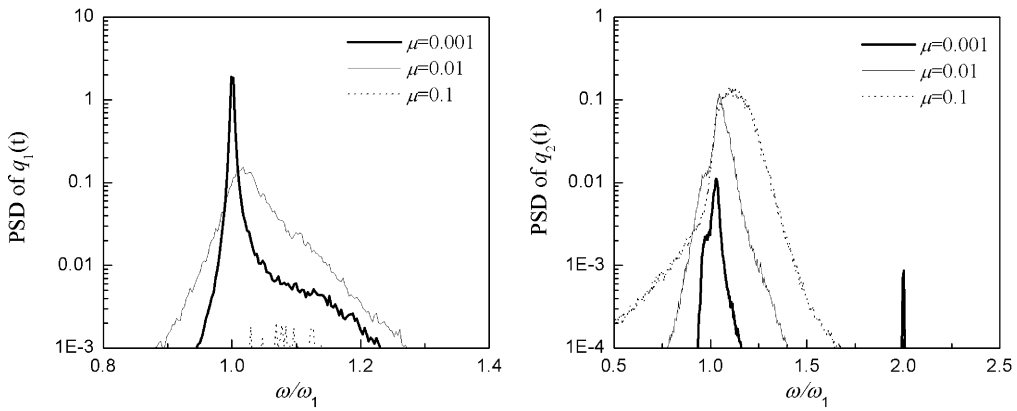

Fig. 16 Stochastic chord elongation. PSD of displacement response at the mid-point. $e_0 = 0.30$, $\omega_0/\omega_1 = 2$

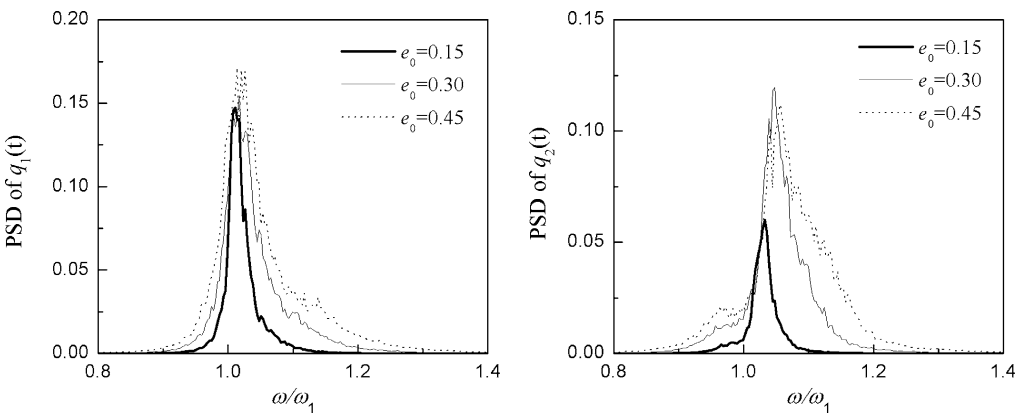

Fig. 17 Stochastic chord elongation. PSD of displacement response at the mid-point. $\mu = 0.01$, $\omega_0/\omega_1 = 2$

and variable values of the characteristic amplitude of the excitation. As seen both the peak frequency and the half-band width of the spectra are increasing with e_0.

Finally, the probability density functions (PDF) of $q_1(t)$ and $q_2(t)$ have been shown in Fig. 18 for $e_0 = 0.30$. As μ approaches the bifurcation value $\mu_c(e_0)$, the PDF of $q_1(t)$ converge towards a Dirac's delta function.

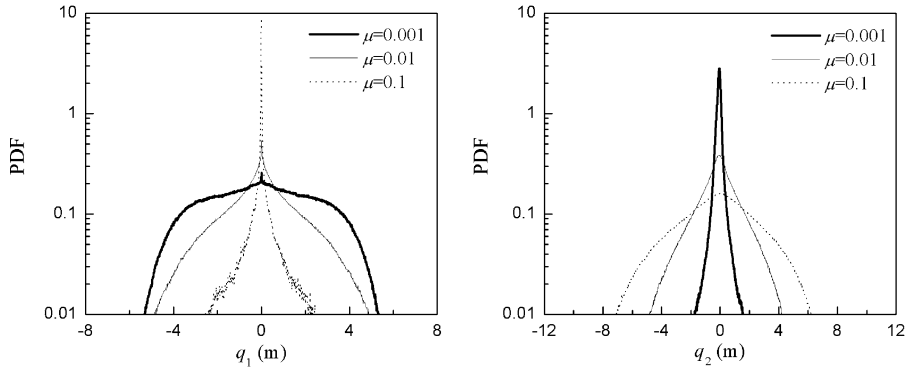

Fig. 18 Stochastic chord elongation. PDF of displacement response at the mid-point. $e_0 = 0.30$, $\omega_0/\omega_1 = 2$

Further it is noticed that $q_1(t)$ and $q_2(t)$ are far from being normally distributed for any of the considered values of μ. This suggests that the variance response of the system may be difficult to be obtained by moment methods, such as equivalent linearization (Gaussian closure), cumulant neglect closure, etc. [14]. Such methods are based on an implicit assumed joint probability density function, which may be considered as an asymptotic expansion from the joint Gaussian distribution obtained exactly in the linear case. At least, the authors tried unsuccessfully to obtain satisfactory results for the variance response, using a fourth order cumulant neglect closure scheme.

6 Conclusions

The subharmonic response of a shallow cable subjected to support point motions changed qualitatively and quantitatively, when a harmonically varying chord elongation is replaced by a comparable narrow-banded Gaussian elongation process with the same centre frequency as the circular frequency of the harmonic excitation, and the same variance. Under harmonic excitation the stable motion consists of a harmonically varying in-plane component with a static drift, and a large subharmonic out-of-plane component with a locked phase difference to the in-plane harmonic component. It is demonstrated that the slowly varying phase of the stochastic excitation implies that the said phase difference varies slowly with time, causing the trajectory of the displacement component to rotate slowly around the chord line. Hence, a large subharmonic response component will also be present in the in-plane displacement. However, as the excitation becomes more broad-banded, the out-of-plane component ceases to exist, and the stochastic subharmonic becomes entirely in-plane. The bifurcation point of the out-of-plane component from the in-plane response depends on the variance of the excitation process.

Under harmonically varying chord elongations the subharmonic response is non-chaotic for all realistic amplitudes and frequencies of the excitation. However, for stochastic excitation there is a tendency of chaotic response, which has been demonstrated via extreme sensitively on the initial values using the same realization of the chord elongation process in the numerical time integration, and via the sign of a numerical calculated Lyapunov exponent. This effect is further analyzed, when replacing the harmonically excitation with an equivalent periodic signal with same standard deviation and frequency, which changes between two levels of amplitudes. Chaotic vibrations, here verified via Poincaré maps, occur when the high and low amplitude phases are changing sufficiently rapidly. From this it is concluded that the corresponding chaotic behaviour under stochastic excitation is related to the rate of change of the envelope process of the excitation. During stochastic excitation it is shown that the response is predictable at very small and large values of the band width parameter, and that the tendency of chaotic behaviour is enhanced, as the variance of the excitation process is increased.

Finally, it is demonstrated that the analysis of the subharmonic response of a shallow cable may be investigated by a reduced 2DOF model, retaining only the lowest out-of-plane and in-plane modes in the modal expansion of the response. It is also demonstrated that the reduced model and the more involved FD model predict almost identical results for stochastic response

quantities such as displacement variance, probability density functions and auto-spectral density functions. Moreover, both models produce chaotic response simultaneously, and the Poincaré maps in case of periodic excitation display the same fractal pattern.

Appendix A: Eigenmodes and coefficients entering the reduced model

The eigenmodes $\Phi_1(x)$ and $\Phi_2(x)$ are given by, [1, 7]

$$\Phi_1(x) = \sin\left(\pi\frac{x}{l}\right),$$
$$\Phi_2(x) = \frac{\cos\left[\left(\frac{\Omega}{2}\right)\left(1-2\frac{x}{l}\right)\right]-\cos\left(\frac{\Omega}{2}\right)}{1-\cos\left(\frac{\Omega}{2}\right)} \tag{A.1}$$

Then, the following results can be evaluated for the Equations (6) and (7)

$$\alpha = \frac{c_2}{c_2+\lambda^2 a_2^2},$$
$$\beta_1 = \frac{1}{8}\bar{\omega}^2\frac{\lambda^2}{f}a_2\frac{c_1}{b_1},$$
$$\beta_2 = \frac{1}{16}\bar{\omega}^2\frac{\lambda^2}{f}a_2\frac{c_1}{b_2},$$
$$\beta_3 = \frac{3}{16}\bar{\omega}^2\frac{\lambda^2}{f}a_2\frac{c_2}{b_2}$$

$$\gamma_1 = \frac{1}{128}\bar{\omega}^2\frac{\lambda^2}{f^2}\frac{c_1}{b_1}c_1,$$
$$\gamma_2 = \frac{1}{128}\bar{\omega}^2\frac{\lambda^2}{f^2}\frac{c_1}{b_1}c_2, \tag{A.2}$$
$$\gamma_3 = \frac{1}{128}\omega_0^2\frac{\lambda^2}{f^2}\frac{c_2}{b_2}c_1$$

$$\gamma_4 = \frac{1}{128}\bar{\omega}^2\frac{\lambda^2}{f^2}\frac{c_2}{b_2}c_2,\ \eta = 8\bar{\omega}^2 f\frac{a_2}{b_2}$$

where λ^2 denotes the Irvine stiffness parameter, which controls the linear as well as the nonlinear parts of the dynamics [7], and $\bar{\omega}$ denotes the fundamental frequency for the taut cable.

$$\lambda^2 = 64\frac{EA}{H}\frac{f^2}{L_e L},\quad \bar{\omega} = \frac{1}{l}\sqrt{\frac{H}{m}} \tag{A.3}$$

The coefficients in Equation (A.2) are function of the nondimensional frequency Ω as follows:

$$a_1 = \frac{2}{\pi},\quad b_1 = \frac{1}{2},\quad c_1 = \frac{\pi^2}{2},$$
$$a_2 = \frac{\sin\frac{\Omega}{2}-\frac{\Omega}{2}\cos\frac{\Omega}{2}}{\frac{\Omega}{2}\left(1-\cos\frac{\Omega}{2}\right)},$$

$$b_2 = \frac{-3\sin\,\Omega+\Omega(2+\cos\,\Omega)}{2\Omega\left(1-\cos\frac{\Omega}{2}\right)^2},$$
$$c_2 = \frac{\Omega^2-\Omega\sin\,\Omega}{2\left(1-\cos\frac{\Omega}{2}\right)^2} \tag{A.4}$$

Ω is obtained as the lowest positive solution to the transcendental equation

$$\tan\frac{\Omega}{2} = \frac{\Omega}{2}-\frac{4}{\lambda^2}\left(\frac{\Omega}{2}\right)^3 \tag{A.5}$$

Appendix B: Algebraic equations for amplitudes and phases in subharmonic responses

Insertion of (10) into (7) with $q_1(t)\equiv 0$, collecting constant terms, and terms with the common factors $\cos(\frac{\omega_0}{2}t+b_2)$ and $\sin(\frac{\omega_0}{2}t+b_2)$, provides the following algebraic equations for A_2, B_2, and b_2

$$\omega_2^2 A_2+\beta_3\left(A_2^2+\frac{1}{2}B_2^2\right)+\gamma_4\left(A_2^3+\frac{3}{2}A_2B_2^2\right)=0 \tag{B.1}$$

$$\omega\,{}^2_2-\frac{\omega_0^2}{4}+2\beta_3A_2+3\gamma_4\left(A_2^2+\frac{1}{4}B_2^2\right) = -\frac{1}{2}\omega_2^2\alpha e_0\cos\,\Phi_2 \tag{B.2}$$

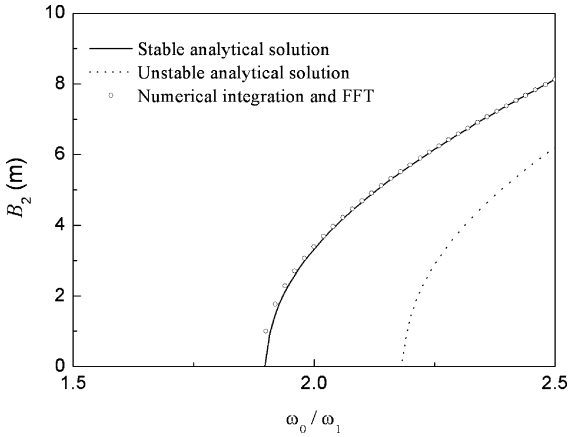

Fig. B1 Subharmonic in-plane response

$$\zeta_2\omega_0\omega_2 = -\frac{1}{2}\alpha\omega_2^2 e_0 \sin\,\Phi_2 \tag{B.3}$$

where $\Phi_2 = a - 2b_2$. (B.3) provides

$$a - 2b_2 = \begin{cases} -\text{Arcsin}\dfrac{2\zeta_2\omega_0}{\alpha e_0\omega_2} \\ \pi - \text{Arcsin}\dfrac{2\zeta_2\omega_0}{\alpha e_0\omega_2} \end{cases} \tag{B.4}$$

Hence, two solutions exist, of which the first indicated turns out to be unstable. Since $\zeta_2 << 1$, the following phase locking prevails for the stable solution, $a - 2b_2 \approx \pi$. The results have been shown in Fig. B1 along with the result obtained via numerical time integration of (7), followed by an FFT.

In the same way insertion of the truncated Fourier expansion (11) into (6) and (7), and collecting constant terms, and terms with the common factors $\cos(\frac{\omega_0}{2}t + b_1)$, $\sin(\frac{\omega_0}{2}t + b_1)$, $\cos(\omega_0 t + c_2)$ and $\sin(\omega_0 t + c_2)$, provides the following algebraic equations for A_2, B_1, C_2, b_1, and c_2.

$$\begin{aligned} &\omega_2^2 A_2 + \frac{1}{2}\beta_2 B_1^2 + \beta_3\left(A_2^2 + \frac{1}{2}C_2^2\right) \\ &\quad + \quad \gamma_3\left(\frac{1}{2}A_2 + \frac{1}{4}\cos\,\Phi_1 C_2\right)B_1^2 \\ &\quad + \quad \gamma_4\left(A_2 + \frac{3}{2}C_2\right)A_2^2 \\ &\qquad = -\frac{1}{2}\omega_2^2\alpha e_0 C_2 \cos\,\Phi_3 \end{aligned} \tag{B.5}$$

$$\begin{aligned} &\omega_1^2 - \frac{\omega_0^2}{4} + \beta_1 A_2 + \frac{3}{4}\gamma_1 B_1^2 + \gamma_2\left(A_2^2 + \frac{1}{2}C_2^2\right) \\ &\quad + \left(\frac{1}{2}\beta_1 + \gamma_2 A_2\right)\cos\,\Phi_1 C_2 \\ &\qquad = -\frac{1}{2}\omega_1^2 e_0 \cos\,\Phi_2 \end{aligned} \tag{B.6}$$

$$\begin{aligned} &\zeta_1\omega_1\omega_0 + \left(\frac{1}{2}\beta_1 + \gamma_2 A_2\right)\sin\,\Phi_1 C_2 \\ &\qquad = -\frac{1}{2}\omega_1^2 e_0 \sin\,\Phi_2 \end{aligned} \tag{B.7}$$

$$\begin{aligned} &\left(\omega_2^2 - \omega_0^2\right)C_2 + 2\beta_3 A_2 C_2 + \frac{1}{2}\gamma_3 B_1^2 C_2 \\ &+\gamma_4\left(3A_2^2 + \frac{3}{4}C_2^2\right)C_2 + \frac{1}{2}\cos\,\Phi_1(\beta_2 + \gamma_3 A_2) \\ &B_1^2 = -\left(\omega_2^2\alpha A_2 + \eta\right)e_0 \cos\,\Phi_3 \end{aligned} \tag{B.8}$$

$$\begin{aligned} &2\zeta_2\omega_2\omega_0 C_2 - \frac{1}{2}\sin\,\Phi_1(\beta_2 + \gamma_3 A_2)B_1^2 \\ &\qquad = -\left(\omega_2^2\alpha A_2 + \eta\right)e_0 \sin\,\Phi_3 \end{aligned} \tag{B.9}$$

where $\Phi_1 = c_2 - 2b_1$, $\Phi_2 = a - 2b_1$, $\Phi_3 = a - c_2 = \Phi_2 - \Phi_1$.

Equations (B.5)–(B.9) must be solved by cyclic iteration. At first (B.6), (B.7) are solved for B_1 and Φ_2. Next, (B.8), (B.9) are solved for C_2 and Φ_3. Finally, A_2 is obtained from (B.5). For the problem shown in Fig. 5, the following solutions are obtained

$$\begin{aligned} &A_2 = -0.105232\,\text{m}, \\ &B_1 = 3.784372\,\text{m}, \\ &C_2 = 0.068925\,\text{m} \\ &\Phi_1 = c_2 - 2b_1 = 3.353320, \\ &\Phi_2 = a - 2b_1 = 3.272428 \end{aligned} \tag{B.10}$$

Acknowledgements The first writer is grateful for the financial support from the Chenguang Project of Wuhan City under Grant 20025001031, and a visiting appointment at Aalborg University, Denmark.

References

1. Nielsen, S.R.K., Kirkegaard, P.H.: Super and combinatorial harmonic response of flexible elastic cables with small sag. J. Sound Vib. **251**, 79–102 (2002)
2. Perkins, N.C.: Modal interactions in the nonlinear response of elastic cables under parametric/external excitation. Int. J. Nonlinear Mech. **27**, 233–250 (1992)
3. Pinto da Costa, A., Martins, J.A.C., Branco, F., Lilien, J.L.: Oscillations of bridge stay cables induced by periodic motions of deck and/or tower. ASCE J. Eng. Mech. **122**, 613–622 (1996)
4. El-Attar, M., Ghobarah, A., Aziz, T.S.: Non-linear cable response to multiple support periodic excitation. Eng. Struct. **22**, 1301–1312 (2000)
5. Rega, G: Nonlinear vibrations of suspended cables-Part II: deterministic phenomena. Appl. Mech. Rev. **57**, 479–514 (2004)
6. Larsen, J.W., Nielsen, S.R.K.: Nonlinear stochastic response of a shallow cable. Int. J. Nonlinear Mech. **41**, 327–344 (2006)
7. Irvine, H.M.: Cable Structure. MIT Press, Cambridge, MA (1981)
8. Zhou, Q., Nielsen, S.R.K., Qu, W.L.: Semi-active control of three-dimensional vibrations of an inclined sag cable with magnetorheological dampers. J. Sound Vib. **296**, 1–22 (2006)
9. Nayfeh, A.H., Mook, D.T.: Nonlinear Oscillations. Wiley, New York (1995)
10. Roberts, J.B., Spanos, P.D.: Random Vibration and Statistical Linearization. Wiley, New York (1990)
11. von Wagner, U., Wedig, W.V.: On the calculation of stationary solutions of multi-dimensional Fokker-Planck equations by orthogonal functions. Nonlinear Dyn. **21**, 289–306 (2000)
12. Clough, R.W., Penzien, J.: Dynamics of Structures. McGraw-Hill, New York (1975)
13. Wolf, A., Swift, J.B., Swinney, H.L., Vastano, J.A.: Determining Lyapunov exponents from a time series. Physica D **16**, 285–317 (1985)
14. Lin, Y.K., Cai, G.Q.: Probabilistic Structural Dynamics: Advanced Theory and Applications. McGraw-Hill, New York (1995)